Boundary-Layer Meteorology (2024) 190:46
https://doi.org/10.1007/s10546-024-00887-5

RESEARCH ARTICLE

Turbulent Heat Fluxes over Arctic Sea Ice: Measurements and Evaluation of Recent Parameterizations

P. Srivastava[1,2] · I. M. Brooks[1] · J. Prytherch[3] · D. J. Salisbury[1] · I. A. Renfrew[4] · A. D. Elvidge[4,5] · M. J. Yelland[6]

Received: 5 June 2024 / Accepted: 1 October 2024

Abstract
We present direct eddy covariance measurements of the surface heat flux in sea ice over a wide range of conditions across the Arctic Ocean made during two research cruises. Photographic imagery of the surface around the ship provides a local, in situ estimate of the ice fraction. Aerodynamically rough conditions prevail for the majority of the time in the consolidated pack ice. The results are analyzed in the framework of a recently-developed parameterization scheme in which the exchange coefficients over ice are functions of a roughness Reynolds number, R_*, hence account for aerodynamic roughness variability. This parameterization accurately represents the measured fluxes under all conditions, while under aerodynamically rough conditions the existing parameterizations from both the Met Office Unified Model, and ECMWF Integrated Forecast System overestimate the fluxes. The results corroborate those of a previous airborne study over the marginal ice zone, and encompass a wider range of atmospheric stability conditions.

Keywords Exchange coefficient · Parameterization · Sea ice · Turbulent heat flux

1 Introduction

The Arctic is warming rapidly, at more than twice the global average rate; a result of multiple feedback processes (Stuecker et al. 2018). A dramatic consequence of this warming is the

M. J. Yelland is retired.

✉ I. M. Brooks
i.m.brooks@leeds.ac.uk

1 School of Earth and Environment, University of Leeds, Leeds LS2 9JT, UK

2 Present Address: Centre of Excellence in Disaster Mitigation and Management, Indian Institute of Technology Roorkee, Roorkee, Uttarakhand 247667, India

3 Department of Earth Sciences, Uppsala University, 751 05 Uppsala, Sweden

4 School of Environmental Sciences, University of East Anglia, Norwich NR4 7TJ, UK

5 Present Address: SSE, Perth PH1 3AQ, Scotland

6 National Oceanography Centre, Southampton SO14 3ZH, UK

Published online: 17 October 2024

substantial reduction in the summer minimum extent of sea ice (Onarheim et al. 2018), and year-round ice thickness and age (Ricker et al. 2017; Kwok 2018); these changes have a strong positive feedback on Arctic climate (Dai et al. 2019). Climate models, while reproducing enhanced warming in the Arctic, show large uncertainties in projected warming (Hodsen et al. 2012) and changes in sea ice (Stroeve et al. 2012, 2014; Zampieri et al. 2018).

A significant source of uncertainty in models is the representation of surface turbulent exchange processes (Bourassa et al. 2013). This can have a significant impact on the representation of both sea ice (Tsamados et al. 2015) and the lower atmosphere (Notz 2012; Renfrew et al. 2019). Parameterisation of turbulent fluxes requires extensive in situ measurements of the surface fluxes themselves, and the environmental parameters that control them, over a wide range of conditions. The sparsity of such measurements over sea ice was demonstrated by Elvidge et al. (2016), who utilized aircraft data from 8 flights over the marginal ice zone, obtaining 195 estimates of the drag coefficient—more than doubling the total number of previously published measurements for the MIZ. Recently we have analyzed a data set of 542 direct estimates of the drag coefficient, acquired during two research cruises in the central Arctic ocean, and sampling a wide range of ice conditions (Srivastava et al. 2022). The results were in good agreement with Elvidge et al. (2016).

Both Elvidge et al. (2016) and Srivastava et al. (2022) use the theoretical framework of Lüpkes et al. (2012) in which the neutral drag coefficient, C_{DN}, is expressed as the sum of three components: the skin drags over water ($C_{\mathrm{DN}w}$) and ice ($C_{\mathrm{DN}i}$), weighted by their respective fractional areas, and the form drag against the ice floe (C_{DNf}):

$$C_{DN} = (1 - A)C_{DNw} + AC_{DNi} + C_{DNf}, \tag{1}$$

where A is the ice fraction, note that the subscript N indicates coefficients are defined for neutral stability. Schemes following this approach have recently been implemented in numerical weather prediction (NWP) models such as the Met Office Unified Model (MetUM, Renfrew et al. 2019) and the ECMWF Integrated Forecast System (IFS; Roberts et al. 2018), the Los Alamos Sea Ice Model (CICE; Tsamados et al. 2014), and a regional coupled climate model (HIRHAM–NAOSIM 2.0; Yu et al. 2020). Within NWP models, C_{DNw} is provided by a parameterization for open ocean and is a function of wind speed, C_{DNi} is fixed, and C_{DNf} is typically specified as a simple function of ice fraction. This is sufficient to represent drag across the marginal ice zone; however, variability in C_{DNi} is large and currently unaccounted for in the parameterization schemes typically implemented in weather and climate models (Elvidge et al. 2016; Castellani et al. 2014; Petty et al. 2017).

Elvidge et al. (2021) examined the scalar fluxes of sensible and latent heat over the MIZ, combining measurements from the Fram Strait and Barents Sea made during the ACCACIA project in 2013 (Elvidge et al. 2016), with new measurements made over the Iceland Sea during the IGP project (Renfrew et al. 2019). Comparing the observations with bulk estimates of the fluxes from the parameterization schemes of the MetUM and IFS, driven by the observed mean meteorology, they found a marked difference between the Fram Strait cases, where the parameterizations closely matched the observed fluxes, and the Iceland and Greenland Sea cases, where both parameterization schemes over-estimated the fluxes, the IFS more so than the MetUM.

The source of this discrepancy was explained by examining the two situations in the framework of a surface renewal model, first proposed by Andreas (1987), in which the dominant process controlling scalar fluxes differs between aerodynamically smooth and rough flow. Details of this model are given in Sect. 2.1. The parameterized fluxes agreed with observations where the flow was predominantly aerodynamically smooth (Fram Strait), and disagreed where it was aerodynamically rough (Iceland Sea).

Elvidge et al. (2021) incorporated the Andreas (1987) conceptual model (hereafter A87) for fluxes over sea ice, into the framework of Lupkes et al. (2012) for fluxes over fraction ice, to produce a 'blended A87' scheme. Good agreement between this new scheme and aircraft measurements was found by Elvidge et al. (2021) for both their data sets, and between MetUM simulations with the blended A87 scheme implemented and the IGP measurements in Elvidge et al. (2023). The existing parameterizations for both the MetUM and IFS reproduced the observed fluxes well for the aerodynamically smooth conditions that dominated the ACCACIA observations (Elvidge et al. 2021), but significantly overestimated those for the aerodynamically rough conditions observed during IGP (Elvidge et al. 2021, 2023). All these aircraft measurements were obtained over the marginal ice zone under conditions of cold air outbreaks, with winds blowing from the ice out over the ocean. Consequently, atmospheric surface-layer conditions varied from near neutral, deeper into the ice, to convective, sometimes strongly so, at low ice fractions, but there were no stable conditions with downward heat fluxes.

Here we further test the blended A87 scheme against a large data set of ship-based measurements from two research cruises in the Arctic Ocean. These encompass a much wider range of sea ice conditions than Elvidge et al. (2021): from the MIZ to well within consolidated pack ice, thin first year ice to thick multi-year ice, and melting ice with substantial areas of melt ponds to just forming frazil ice. Plus, our measurements include both stable and unstable conditions, going beyond the conditions used in Elvidge et al. (2021). This study thus provides an independent test of the blended A87 scheme under conditions more representative of those typical over sea ice in the central Arctic Ocean.

2 Methods

2.1 Theoretical Approach

The neutral drag coefficient is related to the roughness length for momentum (z_0) by Monin–Obukhov similarity theory:

$$C_{DN} = \frac{\kappa^2}{\ln\left(z/z_0\right)^2}, \tag{2}$$

where κ is the von Kármán constant, and z is the height at which the exchange coefficient is evaluated. While the neutral exchange coefficient for heat, C_{HN}, is given by:

$$C_{HN} = \frac{\kappa^2}{\ln\left(z/z_0\right)\ln\left(z/z_{0T}\right)}, \tag{3}$$

where z_{0T} is the roughness length for heat. Similar equations apply for other scalar quantities.

In most current weather and climate models, over consolidated sea ice the scalar roughness lengths for heat and moisture are set to be proportional to that for momentum. For example, the MetUM sets the roughness lengths for heat and moisture, $z_{0Ti} = z_{0qi} = 0.2z_{0i}$, while the IFS sets all three equal ($z_{0Ti} = z_{0qi} = z_{0i}$); note the suffix, i, indicates that the roughness length applies over ice. This assumption of a simple proportionality is not supported by field measurements (e.g., Schröder et al. 2003; Andreas 1987; Andreas et al. 2010; Elvidge et al. 2021).

The analysis of Elvidge et al. (2021) employed the theoretical framework of Andreas (1987). This specifies the exchange coefficients over snow and ice surfaces as functions of

the aerodynamic roughness, expressed as a roughness Reynolds number, R_*:

$$R_* = \frac{z_0 u_*}{\nu}, \tag{4}$$

where z_0 is the roughness length, u_* is the friction velocity, and ν is the kinematic viscosity of the surface air flow. A87 employs different theoretical models for scalar exchange in rough and smooth flow regimes. In aerodynamically smooth flow ($R_* \leq 0.135$), turbulent eddies impinging on the surface are in constant motion, and an advective diffusion model is employed; while in aerodynamically rough flow ($R_* \geq 2.5$), with strong winds over a rough surface, air can become trapped for a time between roughness elements extending above the viscous sublayer, and a molecular diffusion model is used. A transition regime is also defined. The ratios of the scalar roughness lengths to that for momentum are functions of R_* (Fig. 8 in A87 or Fig. 4 in Elvidge et al. 2021), so the different models dictate different scalar exchanges.

The A87 scheme has been found to work effectively over consolidated ice and snow surfaces (A87; Andreas et al. 2010; Fitzpatrick et al. 2019; Elvidge et al. 2021) and similar schemes relating z_{0T} to z_0 as a function of a roughness Reynolds number have been evaluated for other surfaces, including grass and crops (Rigden et al. 2017), rough ice (Smeets and van den Broeke), and fenland (Varentsov et al 2023) among others. The A87 scheme applies only to continuous ice or snow surfaces. In order to extend its use to the marginal ice zone and fractional sea ice cover, Elvidge et al. (2021) proposed a blended scheme where A87 is used to define the exchange coefficients over consolidated ice, and an area-weighted average of the coefficient over solid ice and open water is used for the marginal ice zone; thus for heat,

$$C_{HNi} = \frac{\kappa^2}{\ln\left(z/z_{0i}\right)\ln\left(z/z_{0Ti}\right)}, \tag{5}$$

and

$$C_{HN} = (1 - A)C_{HNw} + AC_{HNi}, \tag{6}$$

where the subscripts i and w, indicate values over solid ice and open water respectively, and,

$$z_{0Ti} = z_{0i} f(R_{*i}). \tag{7}$$

Here R_* from (4) is replaced by a parameterised value, R_{*i},

$$R_{*i} = \frac{z_{0i} u_{*i}}{\nu}, \tag{8}$$

where z_{0i} is the roughness length for momentum over solid ice surfaces, and u_{*i} is the friction velocity over ice, in turn parametrized as:

$$u_{*i} = \frac{\kappa U}{\ln\left(z/z_{0i}\right) + \psi}, \tag{9}$$

where U is the mean wind speed at the reference height, z, and ψ is a stability correction function (e.g., Businger et al. 1971; Dyer 1974).

Note that (6) lacks a third term, equivalent to the form drag term at floe-edges in (1). Current NWP models lack any representation of floe-edge effects on scalar fluxes. Lüpkes and Gryanik (2015) suggest a framework for including it, but at the cost of considerable additional complexity and an uncertain benefit. The blended A87 scheme used here essentially modifies the transfer coefficient over ice within the existing framework of scalar flux parameterization in NWP models.

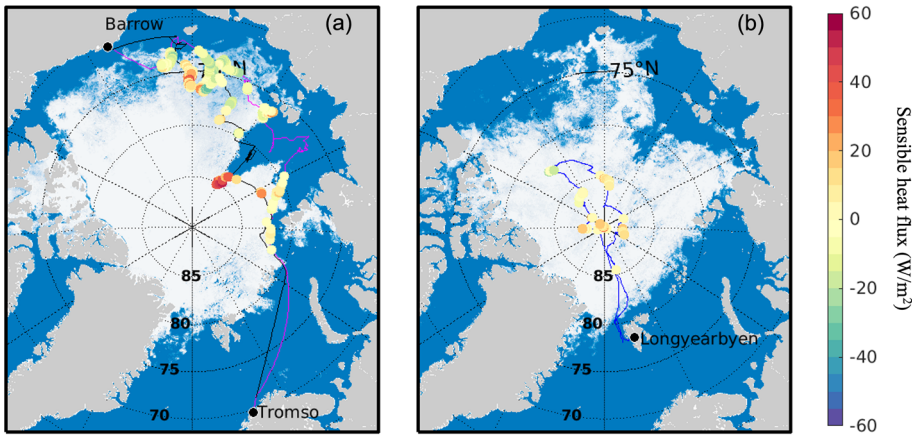

Fig. 1 Maps of the cruise tracks for **a** ACSE and **b** A016. The ice fraction is shown on (a) 07/08/2014 and (b) 07-08-2016. The 30-min mean estimates of turbulent heat flux (positive values indicate an upwards flux) are shown for all points passing the quality control criteria

The exchange coefficient for moisture is defined similarly, but note that the function of $R_{*\mathrm{i}}$ in (7) is defined by A87 to be slightly different for humidity than for heat—a result of the different molecular diffusivities for heat and water vapour (Andreas et al. 1987).

2.2 Measurements

Our measurements are drawn from two research cruises on board the Swedish icebreaker *Oden*. The Arctic Cloud in Summer Experiment (ACSE, Tjernström et al. 2015, 2019; Achtert et al. 2020), was part of the Swedish-Russian-US Arctic Ocean Investigation on Climate-Cryosphere-Carbon (SWERUS-C3), working around the Siberian Shelf between 5 July and 5 October 2014. The Arctic-Ocean 2016 (AO2016) expedition took place between 8 August and 19 September 2016 in the central Arctic Ocean. The cruise tracks are shown in Fig. 1.

Turbulent fluxes were measured via eddy covariance with instruments installed on a mast over Oden's bow, at 20.3 m above the surface. During ACSE the instrumentation consisted of a USA-100 sonic anemometer (Metek GmbH, Elmshorn, Germany) with heated sensing heads and an MTi-700-G motion sensing package (XSENS Technologies B.V., Enschede, Netherlands) installed at the base of the anemometer. The ship's absolute heading and velocity were obtained from its navigation system. During AO2016 the Metek sonic anemometer failed and was replaced with a Gill R3 (Gill Instruments LTD, Lymington, UK). Turbulent quantities were measured at 20 Hz and corrected for platform motion following Edson et al. (1998) and Prytherch et al. (2015, 2017). The mean wind was corrected for the lifting and acceleration of flow that result from distortion induced by the ship using the results of a CFD modelling study (Moat et al. 2015).

Mean temperature and humidity at the mast top were obtained from an aspirated sensor—a MP101 T/RH sensor (Rotronic, Bassersdorf, Switzerland) during ACSE, and a HMP-110 (Väisälä, Vantaa, Finland) during AO2016. Additional measurements of temperature, humidity, and pressure were made by a Väisälä PTU300 sensor on the 7th deck of the ship, 25 m above the surface. Pressure at the mast top was obtained by height-adjusting the measurement from the 7th deck. The surface temperature was measured by two KT15.85-II infra-red surface

temperature sensors (Heitronics, Wiesbaden, Germany) mounted on port and starboard rails of the 7th deck. Networked M24 IP-cameras (Mobotix AG, Langmeil, Germany) mounted alongside the KT15s recorded images of the surface either side of the ship, at 1 min intervals during ACSE, and 15 s intervals during AO2016. Radiosondes (Väisälä RS92) launched every 6 h throughout both cruises provided vertical profiles of the thermodynamic structure of the lower atmosphere, used to asses boundary layer depth. During ACSE additional boundary-layer temperature profiles were obtained every 5 min from a HATPRO scanning microwave radiometer (RPG Radiometer physics GmbH, Meckenheim, Germany), using a manufacturer supplied retrieval tuned to Arctic conditions.

The data used here is from the same data set used to evaluate drag coefficients over sea ice by Srivastava et al. (2022), CO_2 fluxes and transfer velocity by Prytherch et al. (2017), and methane fluxes by Thornton et al. (2020), and shares the same processing and quality control.Turbulent fluxes are estimated over 30-min averaging intervals. Neutral transfer coefficients for drag and sensible heat are calculated from the eddy covariance fluxes, adjusted for stability using the Businger-Dyer stability correction (Businger et al. 1971), and roughness lengths calculated from these via (2). Quality control criteria for stationarity, and well developed turbulence are applied following Foken and Wichura (1996), and for skewness and kurtosis following Vickers and Mahrt (1997), with some additional criteria applied following Srivastava et al. (2022):

- Wind direction relative to the ship was within $\pm$ 120° of the bow.
- Strongly stable or unstable conditions were excluded ($-2 < z/L < 1$; where L is the Obukhov length).
- Mean wind speed > 3 m s^{-1}.
- Cases in very shallow boundary layers, where the measurements on the foremast a Vertical profiles of temperature are likely to be above the Monin–Obukhov surface layer are excluded.

After application of these quality control measures, we retain 631 and 92 data points for the fluxes of heat and momentum from the ACSE and AO2016 campaigns, respectively. The distribution of stabilities is approximately symmetrical about $z/L = 0$, and dominated by near neutral conditions, with 71% of samples having $|z/L| < 0.1$. An open path gas analyzer (Li-7500, LI-COR, Lincoln, Nebraska, USA) was also installed for high frequency humidity measurements, but frequent ice accumulation on the windows meant that too little humidity flux data was retained to carry out a robust analysis.

The local fractions of sea ice and open water were derived for each 30-min flux estimate using the imagery of the surface and the Open Source Sea-ice Processing (OSSP) algorithm of Wright and Polashenski (2018). Images were first quality controlled, with periods where the surface was obscured by fog or ice on the lens, where sun-glint prevented a clear separation of ice and water, or where illumination was poor, were rejected from the analysis. Each image was corrected for lens distortion and cropped to a region from about 20 to 200 m from the ship. A subset of the images representing each surface regime were used to train the OSSP algorithm, with surface types being manually specified. The automated algorithm was then used to process all the images. Finally, the classified images were orthorectified to correct for the oblique viewing angle so that all pixels represent equal areas on the surface. A full description of the image processing procedure is documented in Srivastava et al. (2022). The area of each processed image is approximately 34,225 m^2; the total area imaged within each 30-min averaging interval varies with the number of images passing quality control, and the ship's movement, but is up to approximately 2 km^2 during ACSE and 6.7 km^2 during

AO2016. After excluding periods with poor surface imagery we retain a total of 528 data points, 450 from ACSE, 78 from AO2016.

3 Results

The spatial distribution of the 30-min estimates of sensible heat fluxes for each cruise are shown in Fig. 1, along with representative values for the ice concentration derived from satellite measurements (Spreen et al. 2008). Fluxes are low-to-moderate, as expected for summer, but include both upward and downward heat transfers. Figure 2 shows the ratios of all the individual measurements of the roughness lengths for heat and momentum (z_{0T}/z_0), and roughness length for heat alone (z_{0T}), plotted against R_*, along with binned median values and interquartile and full ranges, for all cases with $A > 0.7$. The results are consistent with those of Elvidge et al. (2021); however, the range of R_* values here is narrower and, in contrast to their measurements over the marginal ice zone, almost all the data here lie within the aerodynamically rough regime.

The absolute magnitudes of the measured heat fluxes (median, interquartile and full ranges) are shown in Fig. 3a, and the transfer coefficients in Fig. 3b, as functions of ice fraction. Also shown are the medians of the parameterized values driven by the observed surface meteorology from the MetUM, IFS, and the blended A87 scheme proposed by Elvidge et al (2021). Again, the results are consistent with those of Elvidge et al. (2021), with the blended A87 scheme providing a close match to the observations, while both MetUM and IFS overestimate the transfer coefficient and magnitudes of the fluxes, IFS more so the MetUM,

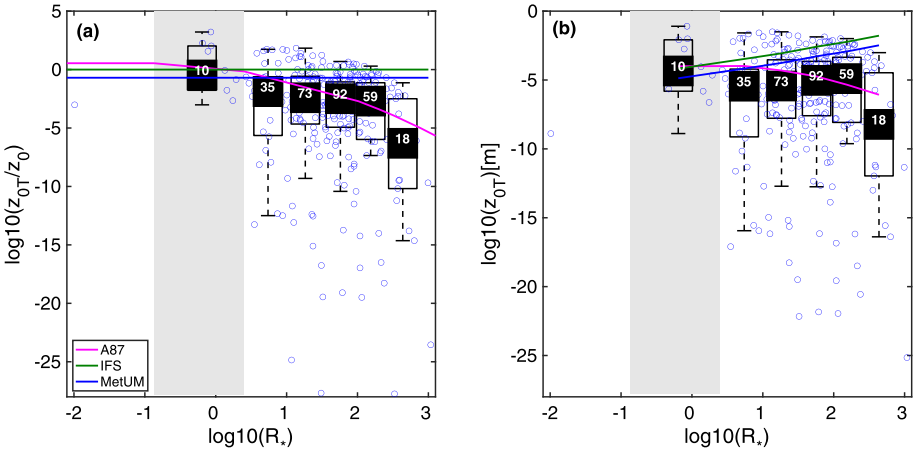

Fig. 2 **a** Ratio of roughness lengths for heat and momentum ($\log_{10}(z_{0T}/z_0)$) as a function of the roughness Reynolds number, R_*, for all measurements with ice fraction $A > 0.7$, plotted against the mean R_* for each bin. **b** Roughness length for heat ($\log_{10}(z_{0T})$) plotted against R_*. Blue circles are from individual 30-min estimates of the roughness lengths; the box and whiskers show median, interquartile range, and full range (excluding outliers). The grey background indicates the *transitional* regime, to the left of this ($R_* < 0.0135$) is the aerodynamically *smooth* regime, and to the right ($R_* > 2.5$) is the aerodynamically *rough* regime. The number of data points within each bin is given at the median. The magenta line is the A87 parameterization driven by the observed R_*, while the blue and green lines are the current parameterizations from the MetUM ($z_{0T}/z_0 = 0.2$) and IFS ($z_{0T}/z_0 = 1$) respectively. In panel (b), the parameterizations use the bin-median observed values of z_0 to calculate z_{0T}

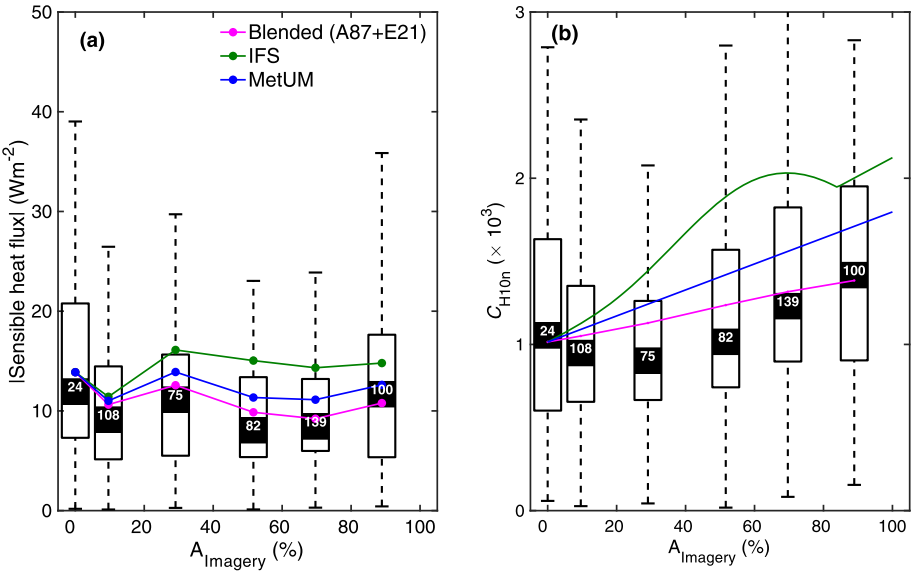

Fig. 3 a The absolute sensible heat flux (|SH|) as a function of ice fraction (the box and whiskers show the median, interquartile range, and range, with the total number of flux estimates indicated). The median is plotted at the mean ice fraction for each bin and the median parameterized values from the blended A87, IFS, and MetUM are overlaid as in the legend. **b** The observed exchange coefficients as a function of ice fraction and the values from the blended A87, IFS, and MetUM parameterizations. Note that the parameterizations in (b) are derived from the end points: the bin median of C_{HW} for $A = 0\%$, and calculated from the bin median for z_{0i} for A = 100%

with median fluxes being almost double those observed for ice fractions of 50–70%. For all ice but the lowest ice fraction, the differences between both the various parameterizations, and between them and the observed values, are larger than the standard error about the median observed fluxes, which range from 1.2 to 2.3 W m^{-2}.

The majority of the measurements here come from the summer melt season or early autumn over pack ice; the magnitudes of the heat flux are modest, rarely exceeding 10–20 W m^{-2}, in contrast to the fluxes in excess of 100 W m^{-2} for low ice fractions observed by Elvidge et al. (2021) in the strongly forced cold air outbreak conditions that dominated their data set.

The very high occurrence of aerodynamically rough conditions in this data set raises the question: how representative are these measurements? Fig. 4 shows the probability of occurrence of different ice fractions, and values of R_* as a function of ice fraction. Ice fraction probability ranges between approximately 6% and 14%, with local maxima at $A \sim 0.1$ and $A \sim 0.7$. There is good representation of all ice fractions. Median values of R_* are all within the rough regime, with a minimum at low ice fractions, increasing to $A = 0.4$, then decreasing very slightly with increasing A (with one higher value for $0.7 < A < 0.8$). The range in R_* does not change markedly with ice fraction.

Figure 5 shows the probability distribution of wind speed for this study compared with other Arctic data sets—MOSAiC measurements for both the whole campaign and July-Sept, and ERA5 for July-Sept of MOSAiC (2020) for all points over sea ice ($A > 15\%$) north of 75°N—and the relationship of R_* with wind speed. The wind speed distributions suggest that our measurements are biased towards slightly higher 10-m wind speeds than typical over the sea ice for this time of year, but are broadly comparable with the full MOSAiC year. The

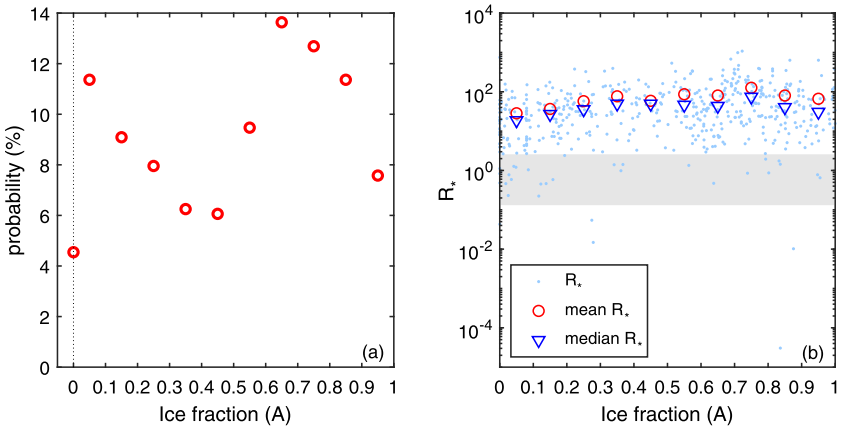

Fig. 4 a Probability distribution of ice fraction, A; **b** individual measurements of R_*, as a function of ice fraction, along with mean and median values in ice fraction bins of width 0.1. The shaded area indicates the transition zone between smooth and rough flow conditions

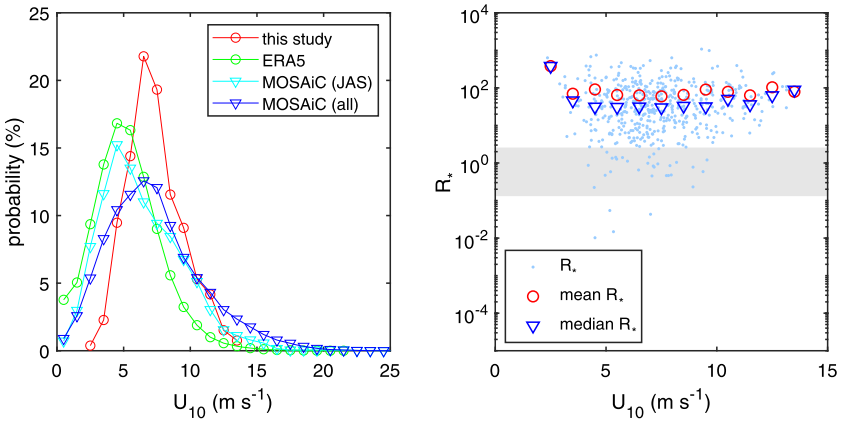

Fig. 5 a Probability distributions of 10-m wind speed for this study, MOSAiC (all data and July/August/September only), and ERA5 for July/August/September 2020 for all ice fractions > 15%. **b** Values of all measurements of R_* with wind speed, along with mean and median values in 1 m s^{-1} wind speed bins

mean and median values of R_* are almost constant with wind speed, increasing slightly only for $U_{10} > 10$ m s^{-1}, where no smooth or transition regime samples occur. This is consistent with the findings of Elvidge et al. (2021, 2023) that R_* has a strong sensitivity to z_0 but only a weak sensitivity to u_* so that the effect of wind speed is of secondary importance.

4 Conclusions

Direct eddy covariance measurements of the turbulent heat flux over Arctic sea ice, obtained during two separate research cruises, have been analyzed in the framework of a new parameterisation scheme (Elvidge et al. 2021). The scheme blends exchange coefficients over ice

and water surfaces, weighted by their respective fractional areas, and over ice the exchange coefficient is a function of the aerodynamic roughness, expressed as a roughness Reynolds number, R_*. Under aerodynamically smooth conditions, scalar roughness lengths are proportional to that for momentum, while under aerodynamically rough conditions the scalar roughness lengths are inversely correlated with that for momentum.

Our results are consistent with those of Elvidge et al. (2021). The blended scheme does a good job of representing the observed fluxes, while the existing schemes from both the MetUM and IFS models, where the scalar roughness lengths are simple multiples of the roughness length for momentum, overestimate the mean heat fluxes by up to approximately 20% and 50% respectively.

Our measurements are obtained much deeper in the pack ice than those of Elvidge et al. (2021), represent all sea-ice fractions and are under conditions of much smaller surface heat fluxes. In contrast to the marginal ice zone measurements of Elvidge et al. (2021), we find that almost all of the data points within the consolidated pack ice lie within the aerodynamically rough regime. The aerodynamically rough conditions dominate at all wind speeds, and all ice fractions, suggesting that this finding is not a result of bias in the conditions sampled. Our findings emphasise the importance of correctly representing aerodynamically rough conditions, where current parameterizations in NWP models will significantly overestimate the scalar fluxes.

Acknowledgements We would like to thank the captains and crew of icebreaker Oden, and the logistics team at the Swedish Polar Research Secretariat for their help throughout the cruises on which our measurements were made. Thanks to Vania López Garcia for providing the ERA5 statistics.

Author Contributions IMB, JP, DS conducted the measurement campaigns, IMB, IAR, MYJ designed the study with input from ADE. JP and DS undertook initial flux data processing, PS processed the surface imagery. PS undertook the analysis with input from all co-authors. IMB and PS wrote the manuscript with input from all co-authors.

Funding This research has been supported by the UK Natural Environment Research Council (NERC) grants NE/S000453/1 and NE/S000690/1. MJY was also supported by NERC grants NE/N018095/1 and NE/V013254/1. The contribution of IMB, JP, and DJS to the ACSE cruise was funded by NERC grant NE/K011820/1. Participation on the AO2016 cruise was supported by the Swedish Polar Research Secretariat. JP was also supported by the Knut and Alice Wallenberg Foundation (Grant 2016-0024).

Data Availability The data used here are publicly available from the Centre for Environmental Data Analysis (CEDA) archives as separate files for each cruise. ACSE cruise data are available at: https://doi.org/10.5285/c6f1b1ff16f8407386e2d643bc5b916a (Brooks et al. 2022a) and the AO2016 data at: https://doi.org/10.5285/614752d35dc147a598d5421443fb50e8 (Brooks et al. 2022b)

Declarations

Conflict of interest The authors declare no competing interests.

References

Achtert P, O'Connor E, Brooks IM, Sotiropoulou G, Shupe MD, Persson POG, Pospichal B, Brooks BJ, Tjernström M (2020) Properties of Arctic mixed phase clouds from ship-borne Cloudnet observations during ACSE 2014. Atmos Chem Phys 20:14983–15002. https://doi.org/10.5194/acp-2020-56

Andreas EL (1987) A theory for the scalar roughness and the scalar transfer coefficients over snow and sea ice. Bound-Layer Meteorol 38(1–2):159–184. https://doi.org/10.1007/bf00121562

Andreas EL, Horst TW, Grachev AA, Persson POG, Fairall CW, Guest PS, Jordan RE (2010) Parametrizing turbulent exchange over summer sea ice and the marginal ice zone. Q J R Meteorol Soc 136(649):927–943. https://doi.org/10.1002/qj.618

Bourassa MA, Gille ST, Bitz C, Carlson D, Cerovecki I, Clayson CA, Cronin M, Drennan W, Fairall C, Hoffman R, Magnusdottir G, Pinker R, Renfrew I, Serreze M, Speer K, Talley L, Wick G (2013) High-latitude ocean and sea ice surface fluxes: challenges for climate research. Bull Am Meteorol Soc 94(3):403–423. https://doi.org/10.1175/BAMS-D-11-00244.1

Brooks IM, Prytherch J, Srivastava P (2022a) CANDIFLOS: surface fluxes from ACSE measurement campaign on icebreaker Oden, 2014. NERC Centre Environ Data Anal. https://doi.org/10.5285/c6f1b1ff16f8407386e2d643bc5b916a

Brooks IM, Prytherch J, Srivastava P (2022b) CANDIFLOS: Surface fluxes from AO2016 measurement campaign on icebreaker Oden, 2016. NERC Centre Environ Data Anal. https://doi.org/10.5285/614752d35dc147a598d5421443fb50e8

Businger JA, Wyngaard JC, Izumi Y, Bradley EF (1971) Flux-profile relationships in the atmospheric surface layer. J Atmos Sci 28:181–189. https://doi.org/10.1175/1520-0469(1971)028%3c0181:FPRITA%3e2.0.CO;2

Castellani G, Lüpkes C, Hendricks S, Gerdes R (2014) Variability of Arctic sea-ice topography and its impact on the atmospheric surface drag. J Geophys Res Oceans 119(10):6743–6762. https://doi.org/10.1002/2013jc009712

Dai A, Luo D, Song M, Liu J (2019) Arctic amplification is caused by sea-ice loss under increasing CO_2. Nature Comms 10(1):121. https://doi.org/10.1038/s41467-018-07954-9

Dyer AJ (1974) A review of flux-profile relationships. Bound-Layer Meteteorol 1:363–372. https://doi.org/10.1007/BF00240838

Edson JB, Hinton AA, Prada KE, Hare JE, Fairall CW (1998) Direct covariance flux estimates from mobile platforms at sea. J Atmos Ocean Technol 15:547–562. https://doi.org/10.1175/1520-0426(1998)0152.0.CO;2

Elvidge AD, Renfrew IA, Weiss AI, Brooks IM, Lachlan-Cope TA, King JC (2016) Observations of surface momentum exchange over the marginal-ice-zone and recommendations for its parameterization. Atmos Chem Phys 16:1545–1563. https://doi.org/10.5194/acp-16-1545-2016

Elvidge AD, Renfrew IA, Brooks IM, Srivastava P, Yelland MJ, Prytherch J (2021) Surface heat and moisture exchange in the marginal ice zone: observations and a new parameterization scheme for weather and climate models. J Geophys Res 126:e2021JD034827. https://doi.org/10.1029/2021JD034827

Elvidge AD, Renfrew IA, Edwards JM, Brooks IM, Srivastava P, Weiss AI (2023) Improved simulation of the Arctic atmospheric boundary layer by accounting for aerodynamic roughness in the parameterisation of surface scalar exchange over sea ice. J Adv Model Earth Syst 15:e2022MS003305. https://doi.org/10.1029/2022MS003305

Fitzpatrick N, Radić V, Menounos B (2019) A multi-season investigation of glacier surface roughness lengths through in situ and remote observation. Cryosphere 13:1051–1071. https://doi.org/10.5194/tc-13-1051-2019

Foken T, Wichura B (1996) Tools for quality assessment of surface based flux measurements. Agr for Meteorol 78:83–105. https://doi.org/10.1016/0168-1923(95)02248-1

Hodson DLR, Keeley SPE, West A, Ridley J, Hawkins E, Hewitt HT (2012) Identifying uncertainties in Arctic climate change projections. Clim Dyn. https://doi.org/10.1007/s00382-012-1512-z

Kwok R (2018) Arctic Sea ice thickness, volume, and multiyear ice coverage: losses and coupled variability (1958–2018). Env Res Letts 13:105005. https://doi.org/10.1088/1748-9326/aae3ec

Lüpkes C, Gryanik VM (2015) stability-dependent parametrization of transfer coefficients for momentum and heat over polar sea ice to be used in climate models. J Geophys Res Atmos 120(2):552–581. https://doi.org/10.1002/2014jd022418

Lüpkes C, Gryanik VM, Hartmann J, Andreas EL (2012) A parametrization, based on sea ice morphology, of the neutral atmospheric drag coefficients for weather prediction and climate models. J Geophys Res 117(D13):D13112. https://doi.org/10.1029/2012jd017630

Moat BI, Yelland MY, Brooks IM (2015) NOC Internal Report 17, National Oceanography Centre, 2015. http://eprints.soton.ac.uk/385311/

Notz D (2012) Challenges in simulating sea ice in earth system models. Wiley Interdiscip Rev Clim Change 3(6):509–526. https://doi.org/10.1002/wcc.189
Onarheim IH, Eldevik T, Smedsrud LH, Stroeve JC (2018) Seasonal and regional manifestation of Arctic Sea ice loss. J Clim 31:4917–4932. https://doi.org/10.1175/JCLI-D-17-0427.1
Petty AA, Tsamados MC, Kurtz NT (2017) Atmospheric form drag coefficients over Arctic sea ice using remotely sensed ice topography data, spring 2009–2015. J Geophys Res Earth Surface 122:1472–1490. https://doi.org/10.1002/2017JF004209
Prytherch J, Yelland MJ, Brooks IM, Tupman DJ, Pascal RW, Moat BI, Norris SJ (2015) Motion-correlated flow distortion and wave-induced biases in air-sea flux measurements from ships. Atmos Chem Phys 15:10619–10629. https://doi.org/10.5194/acp-15-10619-2015
Prytherch J, Brooks IM, Crill PM, Thornton BF, Salisbury DJ, Tjernström M, Anderson LG, Geibel MC, Humborg C (2017) Direct determination of the air-sea CO2 gas transfer velocity in Arctic sea ice regions. Geophys Res Lett. https://doi.org/10.1002/2017GL073593
Renfrew IA, Elvidge AD, Edwards JM (2019) Atmospheric sensitivity to marginal-ice-zone drag: Local and global responses. Q J R Meteorol Soc 145(720):1165–1179. https://doi.org/10.1002/qj.3486
Ricker R, Hendricks S, Kaleschke L, Tian-Kunze X, King J, Haas C (2017) A weekly Arctic sea-ice thickness data record from merged CryoSat-2 and SMOS satellite data. Cryosphere 11:1607–1623. https://doi.org/10.5194/tc-11-1607-2017
Rigden A, Li D, Salvucci G (2017) Dependence of thermal roughness length on friction velocity across land cover types: a synthesis analysis using ameriflux data. Agric for Meteorol 249:512–519. https://doi.org/10.1016/j.agrformet.2017.06.003
Roberts CD, Senan R, Molteni F, Boussetta S, Mayer M, Keeley SP (2018) Climate model configurations of the ECMWF integrated forecasting system (ECMWF-IFS cycle 43r1) for HighResMIP. Geosci Model Dev 11(9):3681–3712. https://doi.org/10.5194/gmd-11-3681-2018
Schröder D, Vihma T, Kerber A, Brümmer B (2003) On the parameterization of turbulent surface fluxes over heterogeneous sea ice surfaces. J Geophy Res 108(C6):3195. https://doi.org/10.1029/2002JC001385
Smeets CJPP, van den Broeke MR (2008) The parameterisation of scalar transfer over rough ice. Boundary-Layer Meteorol 128:339–355. https://doi.org/10.1007/S10546-008-9292-Z
Spreen G, Kaleschke L, Heygster G (2008) Sea ice remote sensing using AMSR-E 89-GHz channels. J Geophys Res 113:C02S03. https://doi.org/10.1029/2005JC003384
Srivastava P, Brooks IM, Prytherch J, Salisbury DJ, Elvidge AD, Renfrew IA, Yelland MJ (2022) Ship-based estimates of momentum exchange coefficient over sea ice and recommendation for its parameterization. Atmos Chem Phys 22:4763–4778. https://doi.org/10.5194/acp-22-4763-2022
Stroeve JC, Kattsov V, Barrett A, Serreze M, Pavlova T, Holland M, Meier WN (2012) Trends in Arctic sea ice extent from CMIP5, CMIP3 and observations. Geophys Res Lett 39:L16502. https://doi.org/10.1029/2012GL052676
Stroeve JC, Hamilton L, Bitz C, Blanchard-Wigglesworth E (2014) Predicting September sea ice: ensemble skill of the SEARCH sea ice outlook 2008–2013. Geophys Res Lett 41:2411–2418. https://doi.org/10.1002/2014GL059388
Stuecker MF, Bitz CM, Armour KC, Proistosescu C, Kang SM, Xie S-H, Kim D, McGregor S, Zhang W, Zhao S, Cai W, Dong Y, Jin F-F (2018) Polar amplification dominated by local forcing and feedbacks. Nature Clim Change 8:1076–1081. https://doi.org/10.1038/s41558-018-0339-y
Thornton BF, Prytherch J, Andersson K, Brooks IM, Salisbury D, Tjernström M, Crill PM (2020) Shipborne eddy covariance observations of methane fluxes constrain Arctic sea emissions. Sci Adv 6:eaay7934. https://doi.org/10.1126/sciadv.aay7934
Tjernström M, Shupe MD, Brooks IM, Persson POG, Prytherch J, Salisbury DJ, Sedlar J, Achtert P, Brooks BJ, Johnston PE, Sotiropoulou G, Wolfe D (2015) Warm-air advection, air mass transformation and fog causes rapid ice melt. Geophys Res Lett. https://doi.org/10.1002/2015GL064373
Tjernström M, Shupe MD, Brooks IM, Achtert P, Prytherch J, Sedlar J (2019) Arctic summer air-mass transformation, surface inversions and the surface energy budget. J Clim 32(3):769–789. https://doi.org/10.1175/JCLI-D-18-0216.1
Tsamados M, Feltham DL, Schroeder D, Flocco D, Farrell SL, Kurtz N, Laxon SW, Bacon S (2014) Impact of variable atmospheric and oceanic form drag on simulations of Arctic sea ice. J Phys Oceanogr 44(5):1329–1353. https://doi.org/10.1175/jpo-d-13-0215.1
Tsamados M, Feltham DL, Petty A, Schroeder D, Flocco D (2015) Processes controlling surface, bottom and lateral melt of Arctic sea ice in a state of the art sea ice model. Phil Trans R Soc A 373:20140167. https://doi.org/10.1098/rsta.2014.0167
Varentsov AI, Zilitinkevich SS, Stepanenko VM, Tyuryakov SA, Alekseychik PK (2023) Thermal roughness of the fen surface. Boundary-Layer Meteorol 187(1–2):213–227. https://doi.org/10.1007/s10546-022-00741-6

Vickers D, Mahrt L (1997) Quality control and flux sampling problems for tower and aircraft data. J Atmos Oceanic Technol 14:512–526.

Wright NC, Polashenski CM (2018) Open-source algorithm for detecting sea ice surface features in high resolution optical imagery. Cryosphere 12:1307–1329. https://doi.org/10.5194/tc-12-1307-2018

Yu X, Rinke A, Dorn W, Spreen G, Lüpkes C, Sumata H, Gryanik VM (2020) Evaluation of Arctic sea ice drift and its dependency on near-surface wind and sea ice conditions in the coupled regional climate model HIRHAM–NAOSIM. Cryosphere 14:1727–1746. https://doi.org/10.5194/tc-14-1727-2020

Zampieri L, Goessling HF, Jung T (2018) Bright prospects for Arctic sea ice prediction on subseasonal time scales. Geophys Res Lett 45:9731–9738. https://doi.org/10.1029/2018GL079394